Elastic and nonlinear acoustic properties of the terbium iron garnet $Tb_3Fe_5O_{12}$ in relation to those of other garnets

G. A. Saunders, S. C. Parker, and N. Benbattouche
School of Physics and Chemistry, University of Bath, Claverton Down, Bath BA2 7AY, United Kindgom

H. L. Alberts
Physics Department, Rand Afrikaans University, P.O. Box 524, Johannesberg, South Africa
(Received 3 December 1991; revised manuscript received 16 March 1992)

The elastic behavior as a function of temperature, pressure, and magnetic field of the ferrimagnetic rare-earth garnet $Tb_3Fe_5O_{12}$, in which all the cation sites are occupied by magnetic ions, has been examined experimentally using the ultrasonic pulse overlap technique. The effects on the ultrasonic wave velocities of a magnetic field applied in a fourfold direction have been measured; that for the [001] polarized shear wave propagated in the [110] direction (and thus for the shear modulus C_{44}) is found to be much larger than for the other ultrasonic modes. Elastic constant determinations made on both sides of the Néel temperature T_N (550±10) K indicate that the magnetic contributions to the elastic stiffnesses are small, being only $\Delta C_{11}/C_{11}\sim 1.0\%$, $\Delta C_{44}/C_{44}\sim 1.3\%$, $\Delta C_L/C_L$ [where $C_L=(C_{11}+C_{12}+2C_{44})/2$] $\sim 1.0\%$. The hydrostatic pressure derivatives of the components of the elastic stiffness tensor constants have been measured at room temperature as $(\partial C_{11}/\partial P)_{P=0}=7.96$, $(\partial C_{44}/\partial P)_{P=0}=1.1$, $(\partial C'/\partial P)_{P=0}=1.55$ [where $C'=(C_{11}-C_{12})/2$] and that of the bulk modulus $(\partial B^S/\partial P)_{P=0}=5.8$. These hydrostatic pressure derivative results have been used to determine the vibrational anharmonicity of the long-wavelength acoustic phonons in terms of the acoustic mode Grüneisen parameters. The mean acoustic mode Grüneisen parameter γ^{el} (=1.36) for $Tb_3Fe_5O_{12}$ is substantially greater, probably due to a magnetic contribution, than those of the other previously investigated garnets $Y_3Al_5O_{12}$ ($\gamma^{el}=0.727$) and $Y_3Fe_5O_{12}$ ($\gamma^{el}=0.885$). To provide a basis for comparison of the elastic behavior of terbium iron garnet with those of other garnets, the elastic stiffness tensor components, their hydrostatic pressure derivatives and associated lattice dynamical properties, including the thermodynamic γ^{th} and mean long-wavelength acoustic γ^{el} Grüneisen parameters and their hydrostatic pressure derivatives, have been calculated for a substantial number of garnet crystals on the basis of the atomistic Born model of solids in which a potential model represents the interionic interactions in the crystal.

I. INTRODUCTION

To determine the elastic behavior of the ferrimagnetic crystal terbium iron garnet ($Tb_3Fe_5O_{12}$), the dependences of ultrasonic-wave velocities upon temperature, pressure, and magnetic field have been measured. $Tb_3Fe_5O_{12}$ has the cubic, garnet structure (space group 0^{10}-$Ia3d$), a useful description of which has been given by Gilleo.[1] There are 8 formula units and, hence, a total of 160 atoms in the garnet structure. Three types of sites are available for cation occupation: a (octahedral, 16 per unit cell), d (tetrahedral, 24), c (skewed cube, 24). Site locations are denoted by $\{P_2\}[Q_2]\{R_3O_{12}\}$, where ions P occupy c sites Q,a and R,d. In $Tb_3Fe_5O_{12}$ the rare-earth ion occupies the c sites and the ferric ions both a and d sites so that there are magnetic ions on each cation site. The five ferric ions in the formula are located such that three Fe^{3+} are on one sublattice (d sites) with magnetization (M_a) in one sense, while the other two are on the second available sublattice (a sites) with magnetization (M_d) in the opposite sense due to a strong a-d exchange interaction. A weaker exchange between the trivalent terbium ions Tb^{3+} and the ferric ions results in the c-sublattice magnetization (M_c) being antiparallel to (M_d-M_a). The overall magnetic interaction depends mainly on the Fe^{3+} interactions rather than on those of Tb^{3+}. The easy direction of magnetization is [111]. At the compensation temperature T_c, which at 244±2 K is much lower than T_N, the bulk magnetization $\{(M_d-M_a)-M_c\}$ disappears.[2] Since $Tb_3Fe_5O_{12}$ is ferrimagnetic, it should more strictly be assigned to a Shubnikov group when it is below its Néel temperature T_N (550±10 K) and consequently is spontaneously magnetized. As well as being of practical importance, the magnetic behavior and associated magnetoelastic effects of the rare-earth garnets have considerable fundamental interest. $Tb_3Fe_5O_{12}$ has remarkable magnetoelastic properties.[2-4] Its magnetostriction is extremely anisotropic.[5,2,6] Below 100 K there is a transition to a rhombohedral form[7] and the accompanying magnetostriction is the largest observed in a rare-earth garnet.[8] Understanding of the magnetoelastic effects requires knowledge of the elastic constants and their temperature, magnetic field, and pressure dependences. The elastic constants of $Tb_3Fe_5O_{12}$ have been measured previously.[9] Intricate behavior of the elastic properties as a function of temperature between 4 and 300 K has been observed and ascribed to the combined effects of the appearance of a double-umbrella magnetic structure and a rhombohedral lattice distortion that sets in below the compensation temperature.[10] On cooling

below 50 K, there is a marked increase in all three elastic stiffness tensor components which may be related to a sharp rise in spontaneous magnetostriction below about 80 K (Ref. 7) and to the evolution of the nonlinear magnetic structure below this temperature.[2] In ferrimagnetic insulators such as the rare-earth garnets, there can be strong-coupling effects between acoustic and spin-wave modes. For $Tb_3Fe_5O_{12}$ this produces a field dependence of the resonant frequency and the acoustic Q of long-wavelength acoustic modes in single-domain samples.[11]

One objective of the present work has been to assess the magnitude of the magnetic contribution to the elastic stiffness tensor components of $Tb_3Fe_5O_{12}$. This has been tackled in two ways: (i) measurement of the dependences of ultrasonic-wave velocities upon magnetic-field strength and direction and (ii) determination of the elastic constants as a function of temperature up to and above the Néel temperature. The measurements of the hydrostatic pressure derivatives of the elastic stiffness tensor components provide parameters necessary to evaluate magnetoelastic effects. In general, these pressure derivatives define the vibrational anharmonicity of the long-wavelength acoustic modes and hence enter into the theoretical description of all nonlinear acoustic and inelastic phenemena.

It is germane to compare the elastic properties of $Tb_3Fe_5O_{12}$ with those of other garnets as this can help resolve some basic questions about the elasticity and its relationship to interatomic binding forces across the compound series. Only for yttrium iron garnet ($Y_3Fe_5O_{12}$) (YIG),[12] which is also ferrimagnetic, and yttrium aluminum garnet ($Y_3Al_5O_{12}$) (YAG) (Ref. 13) and an almondite-pyrope gemstone,[14] which are not, have the pressure dependences of the elastic stiffness tensor components been measured. However comparison of the detailed knowledge available on the elasticity of these two garnets with that obtained here for $Tb_3Fe_5O_{12}$ gives a guide to the effects of magnetic ions. Specific queries include the following: Does the fact that there are no magnetic ions or of d or f electrons in the valence states in YAG result in qualitative differences from YIG and $Tb_3Fe_5O_{12}$ in the interatomic binding and, hence, in elastic or nonlinear acoustic behavior? In the case of $Tb_3Fe_5O_{12}$, does the occupation of the c sites by the magnetic rare-earth ions cause any obvious differences between the properties of YIG and $Tb_3Fe_5O_{12}$? To provide a broad platform for the understanding of the relationships between interionic binding forces, elasticity, and vibrational anharmonicity of acoustic phonons in the long-wavelength limit, the elastic stiffness tensor components, their hydrostatic pressure derivatives, mean long-wavelength acoustic-mode Grüneisen parameters γ^{el}, and thermal Grüneisen parameters γ^{th} have been calculated for a wide range of garnet crystals using an atomistic simulation approach and the results are compared where possible with the sparse experimental available.

II. EXPERIMENTAL PROCEDURE

To examine the crystal perfection, a series of back-reflection x-ray Laue photographs and Debye-Scherrer x-ray powder photographs was taken of the crystals; no indications of regions of different orientation or composition were found. Ultrasonic-wave velocity measurements were made by the pulse-echo overlap technique on a single-crystal specimen having a pair (110) faces polished flat and parallel to better than 10^{-4} rad. Ultrasonic waves were inserted into the specimen using X-cut (for longitudinal modes) and Y-cut (for shear modes) quartz transducers. These were bonded to the crystal using Dow resin 276-V9 for the measurements at room temperature of the effects of pressure and magnetic field on ultrasonic-wave velocities. The hydrostatic pressure dependences of the ultrasonic-wave velocities were measured at pressures up to about 2×10^8 Pa in a piston and cylinder equipment using silicone oil as the pressure-transmitting fluid.[13] The "natural" velocity W (Ref. 15) of the longitudinal and the two shear modes (polarized [001] or [110]) that can be propagated in the [110] direction were found to increase linearly with applied hydrostatic pressure (Fig. 1). The hydrostatic pressure derivatives calculated from the slope $d[\rho_0 W^2]_{P=0}/dP$ and the density ρ_0 at atmospheric pressure using

$$\left[\partial\frac{\rho_0 W^2}{\partial P}\right]_{T,P=0}=\frac{\rho_0 W_0^2}{C_{11}^T+2C_{12}^T}+\left[\frac{d}{dP}[\rho_0 W^2]\right]_{P=0} \quad (1)$$

are given in Table I (together with the hydrostatic pressure derivatives B_{IJ} of the thermodynamic elastic stiffnesses).

Ultrasonic-wave velocities were measured up to 630 K in a thermostatically controlled wire-wound furnace. For these high-temperature measurements, the quartz transducer was bonded to the crystal using Du Pont thick film conductor composition (set by baking at 80 °C for 12 h).

III. EXPERIMENTAL RESULTS FOR $Tb_3Fe_5O_{12}$ AND THEIR INTERPRETATION

A. Effect on the elastic stiffness tensor components of increasing the temperature up through the Néel point

When a ferrimagnetic material is taken through the Néel temperature, there is a change in contribution to the

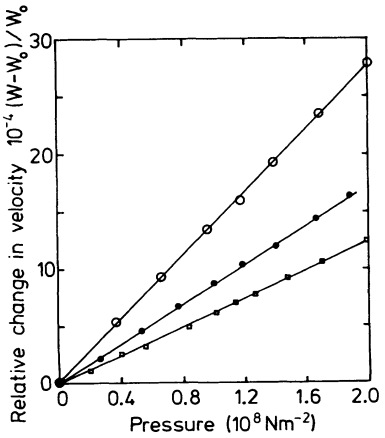

FIG. 1. Relative changes induced by hydrostatic pressure on the "natural" wave velocities of ultrasonic modes with propagation vector **N** directed along the [110] direction in $Tb_3Fe_5O_{12}$ at 291 K; polarization vectors **U**: upper curve [110], middle curve [1$\bar{1}$0], and bottom curve [001].

TABLE I. Elastic properties of garnets. The gemstone is of the almondite-pyrope type and its composition details are given by Soga (Ref. 14).

Material	YIG[a]	YAG[b]	TIG	Gemstone[c]
Density (kg/m^3)	5170	4550	6548	4160
Lattice parameter (Å)	12.376	12.008	12.436	11.531
Elastic stiffness constants (10^{10} N/m^2)				
C_{11}	26.90	32.81	24.53	30.6
C_{12}	10.77	10.64	8.97	11.2
C_{44}	7.64	11.37	7.78	
$C'=(C_{11}-C_{12})/2$	8.06	11.08	7.78	9.7
Anisotropy ratio				
C'/C_{44}	1.055	0.974	1.000	1.04
Bulk modulus B^S (10^{10} N m^{-2})	16.15	18.03	14.15	17.7
Volume compressibility (10^{-12} m^2/N)	0.062	0.055	0.071	0.056
Linear compressibility (10^{-12} m^2/N)	0.020	0.018	0.024	0.019
Elastic compliance constants (!0^{14} m^2/N)				
S_{11}	2.06	1.85	5.10	4.07
S_{12}	−1.400	−0.90	−1.40	−1.1
S_{44}	13.1	8.90	12.9	10.8
$\partial C_{11}/\partial P$	6.22	6.31	7.96	7.48
$\partial C_{12}/\partial P$	4.01	3.51	4.85	4.41
$\partial C_{44}/\partial P$	0.41	0.62	1.1	1.31
$\partial C'/\partial P$	1.10	1.41	1.55	1.54
$\partial B'/\partial P$	4.75	4.44	5.8	5.43
$\partial B^T/\partial P$		4.42		
B_{11}	7.021	7.330	9.50	9.06
B_{12}	2.930	2.520	4.03	5.62
B_{44}	1.354	1.626	2.35	2.48
$C_{111}+2C_{112}$ (10^{11} N/m^2)	−37.640	−42.820	−40.4	−48.1
$C_{144}+2C_{166}$ (10^{11} N/m^2)	−7.600	−8.520	−10.0	−13.2
$C_{123}+2C_{112}$ (10^{11} N/m^2)	−14.670	−15.700	−17.1	−29.9
Debye temperature $\frac{(\mathrm{K})}{\Theta_D^{el}}$	655	708	577	739
Mean Grüneisen parameter gamma $\bar{\gamma}^{el}$	0.885	0.727	1.36	1.24
γ^{th}	0.908	1.43		1.22
Volume thermal expansion (10^{-6} K^{-1})	24.4	22.5	23.5	

[a]Reference 12.
[b]Reference 13.
[c]Reference 14.

total energy and, hence, to the elastic constants arising from the interatomic magnetic interaction. To assess the sign and magnitude of this magnetic contribution to the elastic constants of $Tb_3Fe_5O_{12}$, the velocities of longitudinal modes propagated along the [110] and [001] directions and the [001] polarized shear mode propagated along the [110] direction have been measured from room temperature to just above the Néel temperature ($T_N=568\pm10$ K), above which the magnetically ordered state vanishes.[16] The elastic stiffness tensor components calculated from these data are shown in Fig. 2. In the vicinity of the Néel temperature, there is a moderate elastic stiffening which marks the onset of the paramagnetic state, in which the coupling between the ultrasonic strain and the unaligned magnetic moments must be very weak. When $Tb_3Fe_5O_{12}$ is cooled below T_N, there is only a small reduction in the elastic stiffnesses $\Delta C_{11}/C_{11}\sim1.0\%$, $\Delta C_{44}/C_{44}\sim1.3\%$, and $\Delta C_L/C_L$ [where $C_L=(C_{11}+C_{12}+2C_{44})/2]\sim1.0\%$ as the crystal transforms from the paramagnetic to the ferrimagnetic state.

B. Magnetic-field dependence of the elastic stiffness tensor components

The effective elastic stiffness tensor components C_{IJ} in an applied magnetic field have been determined as $\rho(2L_0/T)^2$ (where L_0 is the specimen length at zero applied field and T is the ultrasonic-wave transit time). Corrections have not been made for the magnetostrictive changes of sample dimensions and density, which are very small at room temperature,[16] that is, substantially above the compensation temperature. The velocity of ultrasonic waves propagated in ferrimagnetic $Tb_3Fe_5O_{12}$ depends upon the magnitude of an applied magnetic field. One difficulty associated with making ultrasonic measurements was that application of the magnetic field led in some experimental configurations to a deterioration of the echo train. Since C_{44} is much the most strongly field-dependent elastic stiffness, the experimental observation that an applied magnetic field up to 0.4 T along the hard direction of magnetization, [100],[17] caused a com-

plete loss of the echoes for the [001] polarized shear wave propagated in the [110] direction was a particular hindrance. Above this value of magnetic field, the echo train was recovered: The loss is possibly due to scattering interactions with the magnetic domain structure, which redistributes with change in the applied field. The dependences of the measured elastic stiffness tensor component combinations C_{11}, C', C_{44}, and $(C_{11}+C_{12}+2C_{44})/2$ upon the magnetic field applied in a $\langle 100 \rangle$ direction are shown in Fig. 3. The fractional increases in C_{11}, C', and $(C_{11}+C_{12}+2C_{44})/2$ and which result from a magnetic-field intensity of about 1.4 T are small, being only +0.6%, +0.7%, and +1.4%, respectively. An applied magnetic-field intensity of only about 0.5 T is required to cause C' to saturate. In contrast, the other shear-mode constant C_{44} does not reach saturation when the field is increased to 1.3 T and has changed by 11% at this applied field; such a change can be considered as large because $Tb_3Fe_5O_{12}$ is a stiff material (that is, it has large elastic stiffness tensor components). The relative changes $\Delta C_{44}/C_{44}$ and $\Delta C_L/C_L$ depend approximately linearly upon $(1/B)$ (Fig. 4). The changes in C' and C_{11} are too small to be satisfactorily fitted to a field dependence. The magnetic-field dependence is largest for the shear elastic mode propagated in the [110] direction and polarized [001], the influence on other long-wavelength phonon modes being much weaker. A qualitative understanding of this observation can be obtained using phenomenological finite-deformation magnetoelasticity theory. The dependences of the velocities of ultrasonic waves propagated in ferrimagnetic crystals upon magnetic-field strength and magnetization orientation should include magnetoelastic contributions to first and second order in strain[18] and contributions from the second-order morphic effect due to magnetostrictive distortion of the crystal.[19] For ultrasonic frequencies well below the spin-wave–phonon crossover frequency, there are no significant contributions from interactions between the acoustic modes and spin waves. An order-of-magnitude assessment of the contribution from the first-order magneto- elastic effect to the magnetic-field dependence of C_{44} has been made for $Tb_3Fe_5O_{12}$. The term in the magnetoelastic energy function for the first-order magnetoelastic effect is

$$U=b_{1111}(a_1^2\eta_{11}+a_2^2\eta_{22}+a_3^2\eta_{33}) + b_{2323}(a_1a_2\eta_{12}+a_2a_3\eta_{23}+a_3a_1\eta_{31}) . \quad (2)$$

Here a_i is the coordinate position and η_{ii} and η_{ij} are Lagrangian strains. The first-order magnetoelastic coefficients b_{2323} and b_{1111} couple components of the magnetic moment to C_{44}-type (η_{ij}, $i \neq j$) and $[(C_{11}-C_{12})/2]$-type ($\eta_{ii}-\eta_{ij}$) strains, respectively. The large magnetic-field effects on C_{44} but small ones on $(C_{11}-C_{12})/2$ result from the fact that, for $Tb_3Fe_5O_{12}$, b_{2323} ($=3\times10^6$ N m^{-2}) is much larger than b_{1111} ($\leq 0.35\times10^6$ N m^{-2}).[20] The magnetic-field-induced change ΔC_{44} in C_{44} for a field applied along the [001] direction can be shown to be

$$\Delta C_{44}=b_{2323}^2/[(B+B_0)M_s] , \quad (3)$$

where B_0 is the total internal flux density. Taking the saturation magnetization M_s of $Tb_3Fe_5O_{12}$ as 0.025 T (Ref. 20) leads to a value of about 6×10^6 N m^{-2} for b_{2323}, about twice that reported previously. The discrepancy probably arises from the neglect in this estimate of the other contributions to ΔC_{44}. However, the observations that C_{44} is the stiffness tensor component most affected and the $(1/B)$ magnetic-field dependence are consistent with the first-order magnetoelastic effect providing the largest contribution to the changes induced in elastic stiffness by an applied magnetic field.

The ultrasonic-wave velocities are dependent also upon the direction of the applied magnetic field. In general,

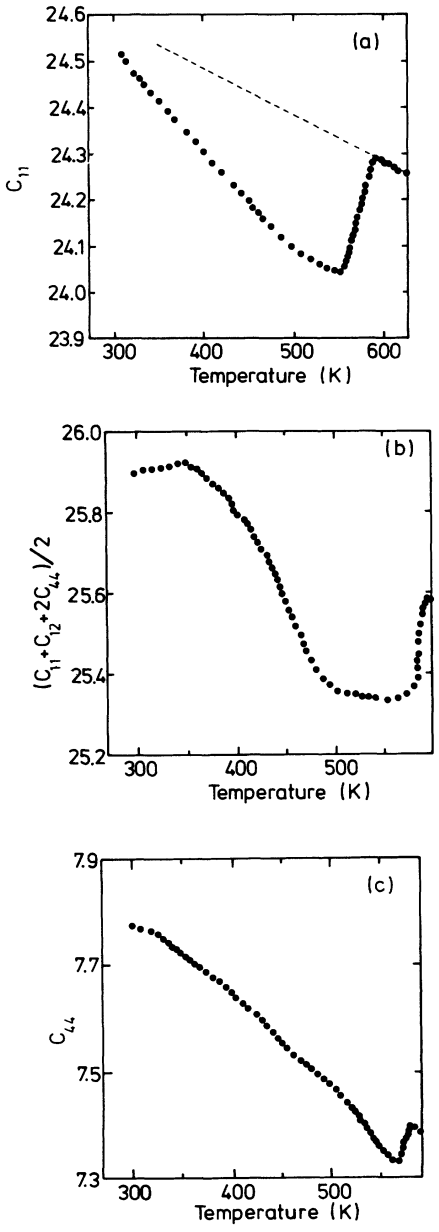

FIG. 2. Dependences of (a) C_{11}, (b) $(C_{11}+C_{12}+2C_{44})/2$, and (c) C_{44} upon temperature up to and beyond the Néel temperature T_N (550±10 K) in $Tb_3Fe_5O_{12}$. Units are 10^{10} N m^{-2}.

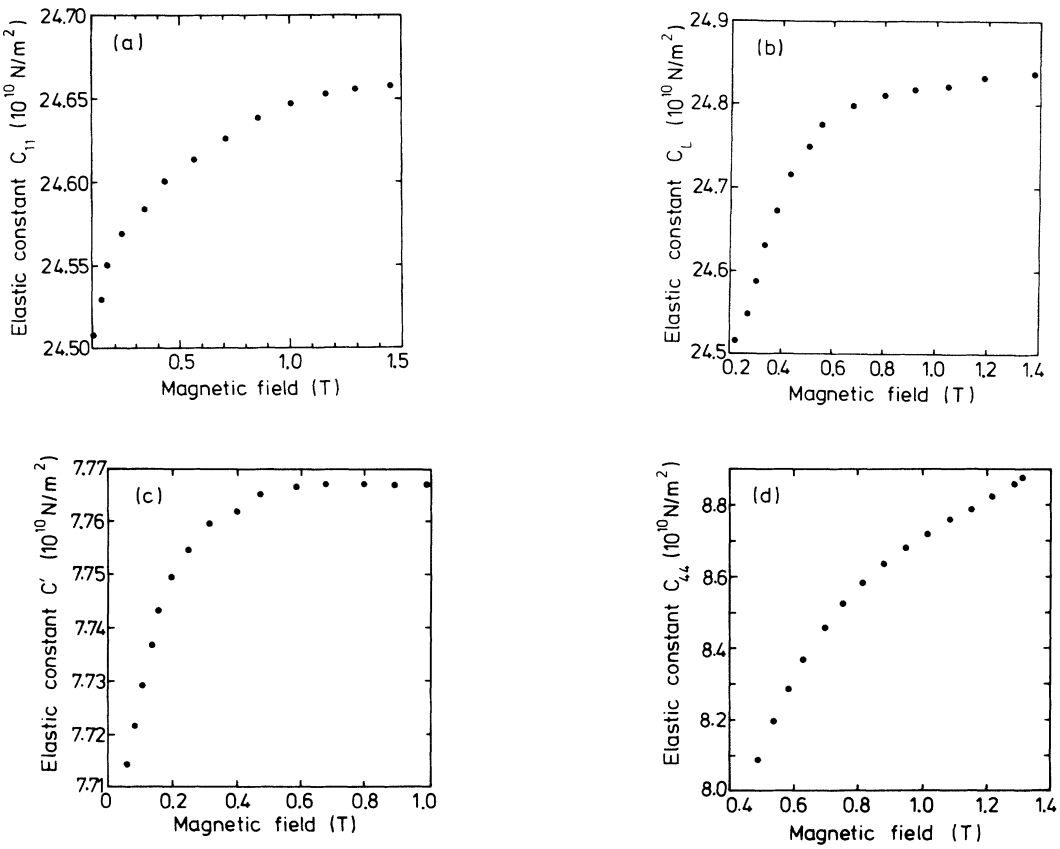

FIG. 3. Dependence of (a) C_{11}, (b) $(C_{11}+C_{12}+2C_{44})/2$, (c) C' $[=(C_{11}-C_{12})/2]$, and (d) C_{44} upon a magnetic field applied in the [100] direction in $Tb_3Fe_5O_{12}$ at 291 K.

the velocities of ultrasonic waves in magnetically saturated ferrimagnetic crystals depend upon magnetic-field strength and direction because of magnetoelastic interactions. For $Tb_3Fe_5O_{12}$ the angular dependence of the shear constant C_{44} is shown in Fig. 5 for three different field intensities (0.65, 0.9, and 1.15 T). The maximum change occurs when the field is applied along a binary $\langle 110 \rangle$ crystallographic direction and the minimum when it is along the hard direction of magnetization (the four-fold direction). When the field is applied along a $\langle 110 \rangle$ direction, the change $\Delta C_{44}/C_{44}$ has become effectively saturated at 0.65 T. At a sufficiently large magnetic field, the ultrasonic-wave velocities and elastic moduli should reach a limiting value. However, further increase of the field results in a small dependence of the magnetization upon the direction of the applied field due to magnetoelastic interactions. For a field applied in a direction at angle θ to the [110] direction, the change in velocity of the shear elastic mode propagated in the [110] direction and polarized [001] due to the first-order magnetoelastic effect is expected to show has a $\cos^2\theta$ orientation dependence,[19] which the C_{44} data (Fig. 5) do follow approximately.

C. Effect of hydrostatic pressure on the elastic stiffness tensor components of $Tb_3Fe_5O_{12}$

While $Tb_3Fe_5O_{12}$ is the least stiff of the garnets whose elastic properties are compared in Table I, its hydrostatic pressure derivatives $(\partial C_{IJ}/\partial P)_{P=0}$ are larger—application of hydrostatic pressure enhances its elastic stiffness more than those of the others, as would be expected. These hydrostatic pressure derivatives provide the first information of an acoustic-mode vibrational anharmonicity of a rare-earth garnet. The anharmonicity of individual acoustic modes at long wavelength can be considered in terms of mode Grüneisen parameters

$$\gamma_i = -\left[\frac{\partial \ln \omega_i}{\partial \ln V}\right]_T . \tag{4}$$

In the anisotropic continuum model, the modes γ_i for a cubic crystal are given by[21]

$$\gamma_i = (1/6w)(3B + 2w + k) , \tag{5}$$

where

$$w = C_{11}K_1 + C_{44}K_2 + C_{12}K_3 , \tag{6}$$

$$k = C_1K_1 + C_2K_2 + C_3K_3 , \tag{7}$$

with

$$K_1 = N_1^2U_1^2 + N_2^2U_2^2 + N_3^2U_3^2 , \tag{8}$$

$$K_2 = (N_2U_3 + N_3U_2)^2 + (N_3U_1 + N_1U_3)^3 + (N_1U_2 + N_2U_1)^2 , \tag{9}$$

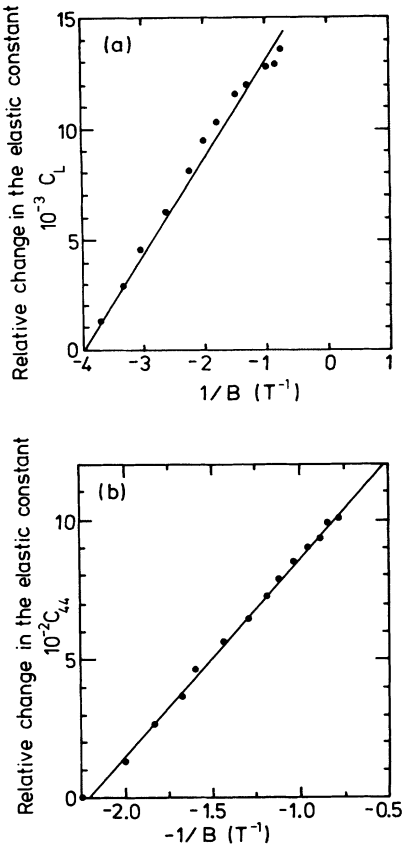

FIG. 4. Relative change ΔC_{IJ} in the elastic stiffnesses (a) $(C_{11}+C_{12}+2C_{44})/2$ and (b) C_{44} upon a magnetic field applied in the [100] direction in $Tb_3Fe_5O_{12}$ at 291 K.

$$K_3=2(N_2N_3U_2U_3+N_3N_1U_3U_1+N_1N_2U_1U_2)\ , \tag{10}$$

$$C_1=C_{111}+2C_{112}\ , \tag{11}$$

$$C_2=C_{144}+2C_{166}\ , \tag{12}$$

$$C_3=C_{123}+2C_{112}\ . \tag{13}$$

Here N_i and U_i are the direction cosines for wave propagation and polarization directions, respectively. The third-order elastic-constant (TOEC) combinations C_1, C_2, and C_3 [Eqs. (11), (12), and (13)] have been obtained from the measurements of the elastic stiffness tensor components and their dependences on pressure given in Table I using

$$(C_{111}+2C_{112})=-\left[2C_{11}+2C_{12}+\{C_{11}+2C_{12}\}\left[\frac{\partial C_{11}}{\partial P}\right]_{P=0}\right], \tag{14}$$

$$(C_{144}+2C_{166})=-\left[C_{11}+2C_{12}+C_{44}+\{C_{11}+2C_{12}\}\left[\frac{\partial C_{44}}{\partial P}\right]_{P=0}\right], \tag{15}$$

$$(C_{123}+2C_{112})=-\left[-C_{11}-C_{12}+\{C_{11}+2C_{12}\}\left[\frac{\partial C_{12}}{\partial P}\right]_{P=0}\right]. \tag{16}$$

The acoustic modes γ_i computed as a function of mode propagation direction in the symmetry planes normal to the twofold and fourfold directions are plotted for $Tb_3Fe_5O_{12}$ in Fig. 6. These should be compared with those for YIG and YAG determined by the same method.[13] For most cubic crystals [including YIG (Ref. 12) and YAG (Ref. 13)], C_{111} is the largest TOEC because it is dominated by nearest-neighbor repulsive forces. Inspection of the TOEC combinations, which can be obtained from the hydrostatic pressure derivatives $(\partial C_{IJ}/\partial P)_{P=0}$ and are given in Table I, suggests that C_{111} is the largest TOEC also in $Tb_3Fe_5O_{12}$. In general, the magnitude of an acoustic-mode Grüneisen parameter is determined by whether a contribution from C_{111} is included in its defining relationship. As an example, the Grüneisen parameters for the two modes which propa-

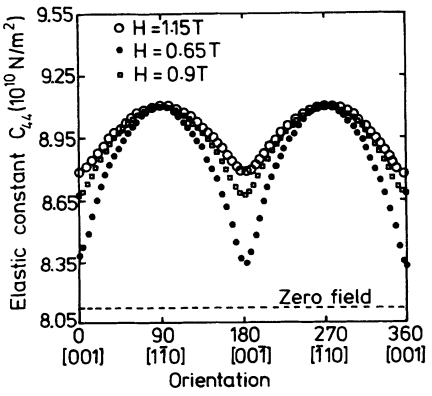

FIG. 5. Dependence of the shear constant C_{44} of $Tb_3Fe_5O_{12}$ at 291 K on the orientation of an applied magnetic field.

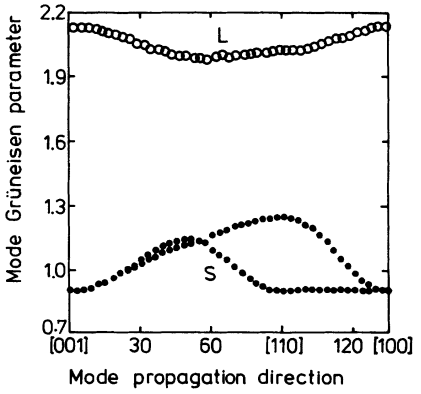

FIG. 6. Zone-center acoustic-mode Grüneisen γ's as a function of propagation direction in $Tb_3Fe_5O_{12}$ at 291 K.

gate along the fourfold ⟨100⟩ direction can be considered. For the longitudinal but not for the shear mode, the Grüneisen parameter involves $(C_{111}+2C_{112})$; hence, the γ_i pertaining to the longitudinal mode is much larger than that for the shear mode (Fig. 6). Physically, the longitudinal-mode Grüneisen parameter is much the larger because it is dominated by the nearest-neighbor repulsive forces. Mode Grüneisen γ's for $Tb_3Fe_5O_{12}$ are substantially larger for all acoustic-mode propagation directions and polarization vectors than those of the other two garnets. As a result, the mean acoustic-mode gamma γ^{el} for $Tb_3Fe_5O_{12}$ is about twice as large as that of YAG and also substantially larger than that of YIG (Table I). Hence the mode anharmonicities, which are related to the pressure-induced changes in the acoustic-phonon frequencies by

$$\gamma_i = -\frac{\partial \ln\omega}{\partial \ln V} , \tag{17}$$

are significantly greater in $Tb_3Fe_5O_{12}$, which has magnetic ions on all three possible cation sites *a*, *c*, and *d*. This indicates stronger intreionic repulsive interactions for ions containing *d* and *f* electrons than for those which do not.

IV. ATOMISTIC MODELING OF THE ELASTIC AND NONLINEAR ACOUSTIC PROPERTIES OF GARNETS

There have been several recent studies that demonstrate that atomistic simulation methods can reliably model the structure and elasticity data of ternary oxides.[22–24] Much of this effort has been stimulated by the need for high-quality elasticity data in mineralogical research, particularly at pressures and temperatures not easily accessible to experiment. The basis of the simulation approach for modeling crystal properties is to start with a trial crystal structure and then adjust the atom positions and cell dimensions until a minimum lattice energy is achieved. The computer model adopted in this study is based on the classical Born model of solids in which the lattice energy is defined as the sum of all the interactions between each pair of ions.

The largest component of the lattice energy arises from the Coulombic interaction as the atoms are assumed to have full ionic charges, i.e., Y^{3+}, Al^{3+}, and O^{2-}; for a discussion on the validity and consequences of this approximation, see Catlow and Stoneham.[25] A second component of the lattice energy results from the short-range energies representing the repulsion between overlapping charge clouds and the attractive van der Waals interaction energies. The short-range term is represented by the simple analytical expression

$$V_{ij}(R_{ij}) = A_{ij}\exp(-R_{ij}/p_{ij}) - C_{ij}/R_{ij}^{-6} , \tag{18}$$

where R_{ij} is the distance between ions *i* and *j*, and *A*, *p*, and *C* are the potential parameters that must be determined for each pair of interactions. The final component of the lattice energy arises from the inclusion of electronic polarizability. This is particularly significant for the highly polarizable O^{2-} ion and is parametrized via the shell model. The choice of these parameters is the key factor in determining the reliability of the simulation. Thus great care must be taken in using a reliable and consistent set of parameters. In this study the potential parameters were fitted empirically to the structure and, where available, elasticity of the component oxides and then transferred to the garnet; e.g., the parameters for YIG were taken from those of Y_2O_3 and Fe_2O_3.[23] This approach has been shown to be successful for calculating structural and elasticity data on minerals.[26,27]

Once the potential model has been identified, the structure can be calculated using energy minimization and the elastic constants determined at the minimized configuration.[28] The pressure dependence was evaluated by recalculating the elastic constants at different applied hydrostatic pressures. The method for calculating the elastic constants under an applied pressure follows the approach adopted by Barron and Klein.[29] Here the elastic constants (defined as the second derivatives of lattice energy with respect to strain) are modified by the effective stress. For example, the elastic constants C_{12} and C_{44} are modified by P_S and $-P_S/2$, respectively, where P_S is the new applied stress.

The elastic stiffness tensor components and their hydrostatic pressure derivatives for a number of rare-earth iron and aluminum garnet crystals (and including those of yttrium and plutonium) determined by the atomistic simulation approach are presented in Tables II and III. Similarities in interatomic binding forces usually result in a general pattern for the second-order elastic constants of crystals. This is so for the rare-earth garnets for which $C_{11} > C_{12} \sim C_{44}$. As would be expected, since the rare-earth ions all have valence 3+ in these compounds and are of similar size, there is little variation between the elastic stiffness tensor components C_{11}, C_{12}, and C_{44} or of the adiabatic bulk modulus B^S (or of their pressure derivatives) over this range of compounds. The model does not include the effects of magnetic contributions to the energy. One of the present aims (Sec. III) has been to measure the size of these magnetic contributions to the elastic constants of $Tb_3Fe_5O_{12}$ so as to provide an indication of how closely the simulation data given in Tables II and III correspond to what values might be expected for the elastic properties of these garnets, as most of them have not yet been studied experimentally. The experimental observation that the magnetic contributions to the elastic stiffnesses of $Tb_3Fe_5O_{12}$ (Fig. 2) are small probably extends to most, if not all, of the ferrimagnetic garnets.

The elastic constants and their pressure derivatives have been measured for YIG (Ref. 12) and YAG (Ref. 13) and now for $Tb_3Fe_5O_{12}$ (Table I). The hydrostatic pressure derivatives $(\partial C_{IJ}/\partial P)$ correspond to third derivatives of the strain-energy function and cannot be expected to be computed theoretically to as high an accuracy as the second-order elastic constants. The theoretical results obtained for $(\partial C_{11}/\partial P)$ and $(\partial C_{44}/\partial P)$ are in reasonable accord with the experimental data, but those of $\partial C_{12}/\partial P$ and, in consequence, $\partial B/\partial P$ (equal to $[\partial(C_{11}+2C_{12})/\partial P]/3$) are much smaller than the experimental values (Table III). For the elastic stiffnesses themselves, which comprise the second derivatives of the strain-energy function, there is as expected more reason-

TABLE II. Properties of rare-earth iron $R_3Fe_5O_{12}$ and aluminum $R_3Al_5O_{12}$ garnets calculated by atomistic simulation. In the first column, R stands for the rare-earth element. γ^{el} is the mean acoustic Grüneisen parameter in the long-wavelength limit, γ_H^{th} is the thermal Grüneisen parameter in the high-temperature limit, and $\gamma_{300\ K}^{th}$ is the thermal Grüneisen parameter at 300 K. Experimental data has been taken from Refs. 12, 14, and 30.

R Fe/Al	Lattice parameter A_0 (Å)	Density ($g\ cm^{-3}$)	Elastic Stiffness (GPa) C_{11}	C_{12}	C_{44}	C'	B_0^S	B_0^T (300 K)	Grüneisen Parameters γ^{el}	γ_H^{th}	$\gamma_{300\ K}^{th}$ 300 K	Specific heat C_p (300 K) $J\,K^{-1}\,atom^{-1}$
90% ionicity												
Lu Fe	12.307 95	7.096	260.5945	82.3276	86.0525	89.133	141.75	140.3728	0.849 770	1.1379	1.279 72	20.478 47
Expt.	12.283											
Yb Fe	12.339 10	7.002	259.203	81.936 01	85.662 07	88.633	141.025	139.7286	0.831 385	1.111 63	1.2465	20.479 98
Expt.	12.302											
Ho Fe	12.417 28	6.702	260.3376	82.140 97	85.4093	89.098	141.54	140.4604	0.785 086	1.036 75	1.150 45	20.448 91
Expt.	12.381											
Y Fe	12.420 66	5.115	260.0786	82.069 33	85.325 68	89.005	141.406	140.3423	0.782 495	1.034 94	1.147 31	20.327 75
Expt.	12.376	5.170	269	107.7	76.4	80.60	161.4		0.885	0.980		
Tb Fe	12.496 11	6.453	259.7539	81.882 18	84.590 89	88.936	141.173	140.2172	0.761 417	0.993 66	1.094	20.441 55
Expt.	12.452	6.548	245.3	89.7	77.8	71.8	141.16		1.36			
Gd Fe	12.526 58	6.372	258.0899	81.471 06	84.036 09	88.309	140.344	139.4179	0.757 277	0.983 62	1.080 84	20.4513
Expt.	12.479		273	125	74		174					
Eu Fe	12.552 68	6.226	258.1298	81.428 91	83.745 01	88.35	140.329	139.4330	0.751 64	0.973 58	1.067 19	20.4448
Expt.	12.518		251	107	74.1		155					
Pu Fe	12.636 41	7.921	256.2857	80.875 51	82.467 76	87.705	139.346	138.5121	0.741 737	0.951 72	1.037 57	20.519 51
Nd Fe	12.654 36	5.925	255.8075	80.740 16	82.170 21	87.534	139.096	138.2792	0.739 285	0.948 28	1.031 97	20.452 94
La Fe	12.795 31	5.63	251.9904	79.674 09	79.6776	86.158	137.113	136.3609	0.731 756	0.932 79	1.007 25	20.4775
Lu Al	11.819 54	6.852	331.0063	104.0583	105.8066	113.474	179.708	178.8034	0.729 397	0.914 72	1.021 32	19.0479
Yb Al	11.849 52	6.754	328.1531	103.4839	104.9536	112.335	178.374	177.4874	0.731 234	0.910 73	1.014 69	19.067 65
Ho Al	11.928 76	6.43	325.3253	102.7605	103.0724	111.282	176.949	176.1028	0.760 485	0.905 82	1.001 92	19.087 48
Y Al	11.932 12	4.641	324.9553	102.6900	102.9708	111.133	176.778	175.9501	0.728 434	0.903 02	0.997 15	18.951 46
Expt.	12.008	4.550	328.1	106.4	113.7	110.8	180.3		0.727	1.43		
Tb Al	12.008 00	6.165	321.1531	101.8269	100.9847	109.663	174.936	174.1223	0.731 773	0.901 73	0.992 15	19.117 76
Gd Al	12.037 61	6.081	318.2077	101.2863	100.1056	108.461	173.594	172.7866	0.737 436	0.902 22	0.991 36	19.139 66
Eu Al	12.064 24	5.921	317.1143	101.0261	99.398 11	108.044	173.056	172.2544	0.738 432	0.903 61	0.991 25	19.144 35
Pu Al	12.148 39	7.845	311.7951	99.974 56	97.010 68	105.91	170.581	169.7827	0.749 734	0.911 27	0.996 57	19.261 09
Nd Al	12.166 43	5.602	310.5878	99.747 25	96.486 72	105.42	170.027	169.2348	0.751 823	0.913 63	0.997 83	19.193 46
La Al	12.308 82	5.296	301.1679	98.086 14	92.230 83	101.541	165.78	164.9685	0.779 302	0.942 06	1.025 61	19.273 88
100% ionicity												
Lu Fe	12.307 95	7.096	321.7028	101.6303	106.2355	110.036	174.988	173.6506	0.849 848	1.119 12	1.281 48	19.855 51
Yb Fe	12.339 13	7.002	319.9869	101.1475	105.7539	109.42	174.094	172.8372	0.831 424	1.092 82	1.247 28	19.859 28
Ho Fe	12.417 29	6.702	321.3883	101.4012	105.4424	109.994	174.73	173.6912	0.785 116	1.017 36	1.147 49	19.830 68
Y Fe	12.420 87	5.115	321.1227	101.3327	105.3637	109.895	174.596	173.5754	0.783 185	1.015 71	1.143 88	19.687 98
Tb Fe	12.496 11	6.453	320.6688	101.0823	104.4324	109.793	174.278	173.3627	0.761 44	0.973 84	1.088 66	19.824 16
Gd Fe	12.526 64	6.372	318.6159	100.5750	103.7470	109.02	173.255	172.3694	0.757 285	0.963 79	1.075 06	19.834 85

TABLE II. (*Continued*).

R Fe/Al	Lattice parameter A_0 (Å)	Density (g cm^{-3})	Elastic C_{11}	Elastic C_{12}	Stiffness (GPa) C_{44}	C'	B_0^S	B_0^T (300 K)	Grüneisen γ^{el}	Parameters γ_H^{th}	$\gamma_{300\text{ K}}^{th}$ 300 K	Specific heat C_p (300 K) J K^{-1} atom^{-1}
Eu Fe	12.552 73	6.226	318.6651	100.5230	103.3878	109.071	173.237	172.3812	0.751 655	0.953 57	1.060 69	19.827 43
Pu Fe	12.636 48	7.921	316.3890	99.840 14	101.8106	108.274	172.023	171.2287	0.741 746	0.931 32	1.029 79	19.914 59
Nd Fe	12.654 43	5.925	315.7988	99.673 14	101.4433	108.063	171.715	170.9386	0.739 286	0.927 81	1.023 57	19.835 05
La Fe	12.795 36	5.63	311.0865	98.357 29	98.366 58	106.365	169.267	168.5557	0.731 764	0.911 67	0.996 87	19.859 01
Lu Al	11.819 53	6.852	408.6348	128.4599	130.6256	140.087	221.852	220.9987	0.729 407	0.893 65	1.013 76	18.317 74
Yb Al	11.849 53	6.754	405.1127	127.7510	129.5720	138.681	220.205	219.3696	0.731 245	0.889 68	1.006 78	18.338 24
Ho Al	11.928 76	6.43	401.6225	126.8582	127.2500	137.382	218.446	217.6516	0.767 923	0.884 79	0.992 76	18.356 15
Y Al	11.932 19	4.641	401.1643	126.7707	127.1227	137.197	218.235	217.4613	0.728 435	0.881 51	0.986 69	18.196 72
Tb Al	12.008 00	6.165	396.4725	125.7060	124.6729	135.383	215.962	215.2006	0.731 788	0.879 86	0.981 21	18.385 62
Gd Al	12.037 66	6.081	392.8348	125.0384	123.5861	133.898	214.304	213.5493	0.737 437	0.880 36	0.980 23	18.408 27
Eu Al	12.064 28	5.921	391.4853	124.7172	122.7129	133.384	213.64	212.8916	0.738 437	0.881 58	0.979 68	18.4117
Pu Al	12.148 44	7.845	384.9176	123.4190	119.7647	130.749	210.585	209.8391	0.749 718	0.888 89	0.984 42	18.541 73
Nd Al	12.166 48	5.602	383.4273	123.1385	119.1179	130.144	209.901	209.1628	0.751 832	0.891 18	0.985 17	18.460 05
La Al	12.308 81	5.296	371.8016	121.0887	113.8660	125.356	204.66	203.9044	0.779 298	0.918 96	1.011 95	18.540 51

able agreement between the theoretical and experimental data (Table II), although the theoretical calculation has somewhat overestimated C_{11}, C_{44}, and the bulk modulus B_0^S in each case by 10–20 %. In order to check the sensitivity of the properties to the details of the potential, the parameters were modified. The approach adopted for modifying the parameters was to adjust the ionicity. This was achieved by modifying the charges on each atom such that the overall stoichiometry remained unchanged and that the nearest-neighbor forces and derivatives were unchanged. The effect of reducing the ionicity to 90% of its full value reduced the second-order elastic constants. The value of 90% was chosen as this produced the best agreement between the calculated and the experimental bulk modulus of $Tb_3Fe_5O_{12}$ (Table II). In contrast to the sensitivity of the second-order elastic constants to the details of the potential model, the pressure derivatives are relatively insensitive. This then gives us confidence in the calculated third derivatives and that the good agreement was not fortuitous.

A feature common to the experimental and calculated elastic constants is that they show that garnets are close to the condition $C_{44}=(C_{11}-C_{12})/2$ for isotropy of the shear moduli. The presence or absence of *d* or *f* electrons in the interatomic bonds does not produce a noticeable influence of the tendency of garnet structure crystals to obey the Cauchy relation $C_{12}=C_{44}$, which is usually taken to indicate interionic interaction through central forces (for the complex garnet structure, even if forces are central, the Cauchy relation need not be rigorously obeyed). In general, the elastic constants for a series of compounds, such as garnets, which are isostructural, have similar ions and also have comparable lattice parameters, would be expected to be alike. This is the case for the iron garnets, which all have much the same C_{11}, C_{12}, C_{44}, and bulk modulus (Table II). It is also true for the aluminum garnets. The iron garnets have smaller elastic constants than those of the aluminum garnets. This may be a result of the rather smaller ionic radius of Al^{3+} (0.53 Å) than that of Fe^{3+} (0.55 Å) or of the large difference in mass between these two ions.

The method for calculating the thermal contributions is based on lattice dynamics. This is an approach for calculating vibrational frequencies in periodic structures. The major limitation of calculations using lattice dynamics is the quasiharmonic approximation, in which the vibrational motions in the solid are assumed to comprise independent quantized harmonic oscillators whose frequencies vary with cell volume. Lattice dynamics currently provides the most efficient method for determining thermodynamic properties and phase stabilities of solids because the technique can rapidly evaluate a range of thermodynamic properties of different structures using sophisticated and reliable interatomic potentials, unlike alternative methods such as molecular dynamics, which cannot yet be routinely applied to systems where electronic polarizability is an important component. The major limitation of this technique is that the atoms in lattice dynamics are held fixed when evaluating vibrational frequencies and, thus, only sample the energy at the specific lattice sites where the shape of the potential ener-

gy well is assumed to be harmonic. Thus this approach requires that anharmonic effects are not significant; this would not be the case when the temperature of the mineral approaches its melting point or if it undergoes a displacive or soft-mode phase transition.

As noted, one measure of the effect of temperature dependence on structural and thermal properties is the Grüneisen parameter, as it links the microscopic properties, namely, the change in frequencies with the macroscopic properties, such as the thermal-expansion coefficient. The thermal Grüneisen parameter can be determined from the change in frequencies with volume directly by first calculating the mode Grüneisen parameters for each frequency using Eq. (17). The acoustic Grüneisen parameter has been calculated by averaging the mode Grüneisen parameters near the zone center.

TABLE III. Properties of rare-earth iron $R_3Fe_5O_{12}$ and aluminum $R_3Al_5O_{12}$ garnets calculated by atomistic simulation. In the first column R stands for the rare-earth element. $\partial\gamma^{el}/\partial P$ is the hydrostatic pressure derivative of the mean acoustic Grüneisen parameter in the long-wavelength limit, $\partial\gamma_H^{th}/\partial P$ is the hydrostatic pressure derivative of the thermal Grüneisen parameter in the high-temperature limit, and $\partial\gamma_{300\ K}^{th}/\partial P$ is the hydrostatic pressure derivative of the thermal Grüneisen parameter at 300 K. Experimental data has been taken from Refs. 12, 13, and 30.

	Pressure derivative of the elastic stiffness						Grüneisen Parameters (GPa^{-1})		
R Fe/Al	$\partial C_{11}/\partial P$	$\partial C_{12}/\partial P$	$\partial C_{44}/\partial P$	$\partial C'/\partial P$	$\partial B^S/\partial P$	$\partial B^T/\partial P$	$\partial\gamma^{el}/\partial P$	$\partial\gamma_H^{th}/\partial P$	$\partial\gamma_{300\ K}^{th}/\partial P$
90% ionicity									
Lu Fe	6.718 509	3.089 436	0.468 509	1.814 545	4.299 090	4.372 090	−0.042 06	−0.044 21	−0.053 63
Yb Fe	6.630 636	3.005 136	0.437 163	1.812 727	4.213 636	4.273 682	−0.038 04	−0.040 21	−0.048 62
Ho Fe	6.522 633	2.879 954	0.332 290	1.820 909	4.094 545	4.121 989	−0.031 44	−0.029 72	−0.035 66
Y Fe	6.513 990	2.871 563	0.330 181	1.821 818	4.085 454	4.113 264	−0.031 23	−0.029 56	−0.035 72
Expt.	6.22	4.01	0.41	1.1	4.44				
Tb Fe	6.442 654	2.7836	0.283 536	1.83	4.003 636	4.018 302	−0.030 62	−0.025 12	−0.029 90
Expt.	7.96	4.85	1.17	1.55	5.86				
Gd Fe	6.405 5	2.734	0.277 490	1.835 454	3.958 181	3.970 673	−0.030 57	−0.024 31	−0.028 84
Eu Fe	6.395 572	2.718 1	0.263 645	1.838 181	3.943 636	3.954 283	−0.030 74	−0.023 4	−0.027 71
Pu Fe	6.360 572	2.654 718	0.235 472	1.852 727	3.89	3.896 153	−0.031 51	−0.021 76	−0.025 49
Nd Fe	6.355 45	2.642 890	0.230 890	1.856 363	3.88	3.886 290	−0.031 58	−0.021 54	−0.025 30
La Fe	6.351 327	2.5817	0.1948	1.884 545	3.838 181	3.841 352	−0.033 20	−0.020 95	−0.024 40
Lu Al	6.295 227	2.575 190	0.210 672	1.86	3.815 454	3.807 610	−0.024 23	−0.016 03	−0.019 70
Yb Al	6.279 80	2.535 145	0.211 272	1.872 727	3.783 636	3.775 986	−0.024 46	−0.015 96	−0.019 53
Ho Al	6.290 663	2.508 872	0.191 663	1.890 909	3.77	3.757 45	0.003 53	−0.013 47	−0.016 83
Y Al	6.288 509	2.503 8	0.191 754	1.892 727	3.764 545	3.757 534	−0.025 24	−0.015 87	−0.019 44
Expt.	6.31	3.51	0.62	1.4	4.44	4.42			
Tb Al	6.304 536	2.476 554	0.179 936	1.913 636	3.752 727	3.745 574	−0.026 16	−0.0162	−0.019 60
Gd Al	6.307 372	2.447 963	0.183 936	1.93	3.734 545	3.728 123	−0.026 54	−0.016 46	−0.019 87
Eu Al	6.318 227	2.445 636	0.179 145	1.936 363	3.737 272	3.730 951	−0.026 87	−0.016 69	−0.020 14
Pu Al	6.354 509	2.418 954	0.176 490	1.967 272	3.73	3.737 601	−0.028 104	−0.017 74	−0.021 30
Nd Al	6.361 818	2.412 981	0.176 436	1.974 545	3.729 090	3.727 021	−0.028 315	−0.018 03	−0.021 72
La Al	6.455 890	2.381 372	0.182 290	2.032 737	3.736 363	3.741 508	−0.030 939	−0.021 21	−0.025 58
100% ionicity									
Lu Fe	6.707 872	3.093 972	0.459 518	1.806 363	4.299 090	4.349 504	−0.033 635	−0.035 35	−0.044 07
Yb Fe	6.619 872	3.010 009	0.429 290	1.805 454	4.213 636	4.253 729	−0.030 514	−0.032 18	−0.04
Ho Fe	6.510 809	2.885 163	0.327 063	1.813 636	4.093 636	4.108 921	−0.025 354	−0.023 90	−0.029 44
Y Fe	6.503 763	2.877 455	0.326 090	1.812 727	4.086 363	4.101 231	−0.025 178	−0.023 77	−0.029 52
Tb Fe	6.429 936	2.788 863	0.278 954	1.82	4.002 727	4.007 858	−0.024 708	−0.020 25	−0.024 72
Gd Fe	6.392 718	2.739 345	0.273 054	1.826 363	3.957 272	3.960 797	−0.024 664	−0.019 59	−0.023 84
Eu Fe	6.382 490	2.723 409	0.259 327	1.829 090	3.942 727	3.944 827	−0.024 788	−0.018 86	−0.022 9
Pu Fe	6.346 863	2.659 972	0.231 345	1.842 727	3.889 090	3.887 496	−0.025 406	−0.017 55	−0.021 03
Nd Fe	6.341 618	2.648 136	0.226 309	1.847 272	3.879 090	3.877 715	−0.025 474	−0.017 37	−0.0209
La Fe	6.336 554	2.586 754	0.190 790	1.875 454	3.836 363	3.832 917	−0.026 769	−0.0169	−0.020 11
Lu Al	6.284 736	2.579 181	0.2076	1.852 727	3.814 545	3.800 124	−0.019 560	−0.012 95	−0.016 37
Yb Al	6.269 245	2.539 145	0.2082	1.865 454	3.782 727	3.768 602	−0.019 739	−0.012 89	−0.016 21
Ho Al	6.279 954	2.512 927	0.1887	1.883 636	3.768 181	3.749 769	0.015 167	−0.009 97	−0.013 08
Y Al	6.277 481	2.507 690	0.188 681	1.885 454	3.763 636	3.750 104	−0.020 367	−0.012 80	−0.016 14
Tb Al	6.293 109	2.480 336	0.176 863	1.906 363	3.751 818	3.737 935	−0.021 089	−0.013 05	−0.016 22
Gd Al	6.295 872	2.451 736	0.180 827	1.921 818	3.733 636	3.720 383	−0.021 413	−0.013 26	−0.016 43
Eu Al	6.306 581	2.449 372	0.176 027	1.928 181	3.735 454	3.723 062	−0.021 674	−0.013 44	−0.016 64
Pu Al	6.342 718	2.422 672	0.173 318	1.96	3.729 090	3.719 257	−0.022 668	−0.014 28	−0.017 55
Nd Al	6.349 709	2.416 636	0.1732	1.966 363	3.727 272	3.718 398	−0.022 820	−0.014 50	−0.017 91
La Al	6.433 045	2.384 954	0.1788	2.023 636	3.734 545	3.731 160	−0.024 931	−0.017 03	−0.021 04

The high-temperature thermal Grüneisen parameter includes contributions from all the modes, both acoustic and optic, and these have been taken into consideration.

The bulk or thermal Grüneisen parameter γ^{th} has been evaluated by taking the average of the heat-capacity weighted mode Grüneisen parameter

$$\gamma_i = \frac{1}{C_V} \sum C_i \gamma_i \ , \tag{19}$$

where C_i is the contribution to the total heat capacity of mode i.

Comparison between the Grüneisen parameters γ^{el} and γ^{th} of the different garnets given in Table III shows them to be parameter insensitive. Greater vibrational anharmonicity of the iron garnets is implied by their consistently larger Grüneisen-parameter values than those of the aluminum garnets. The calculated mean acoustic Grüneisen parameters γ^{el} are all between 0.7 and 0.9. While the theoretical value of γ^{el} determined for YAG, which does not contain magnetic ions, is in excellent agreement with that determined experimentally, it is somewhat smaller for YIG. In the case of $Tb_3Fe_5O_{12}$, in which the Tb^{3+} ion occupies each c site and the ferric ions both a and d sites so that there are magnetic ions on each cation site, the theoretical γ^{el} is far lower than the experimental quantity. These findings suggest that an important contribution may be missing from the potential, particularly given the insensitivity to changes in the potential parameters. One such contribution is, of course, the magnetic contribution.

V. CONCLUSIONS

(i) The second-order elastic stiffness tensor components of $Tb_3Fe_5O_{12}$ are somewhat smaller and their hydrostatic pressure derivatives $(\partial C_{IJ}/\partial P)_{P=0}$ and $(\partial B^S/\partial P)_{P=0}$ are rather larger than those of YIG and YAG (Table I).

(ii) The second-order elastic stiffness tensor components of $Tb_3Fe_5O_{12}$ decrease by a small amount as its temperature is reduced through T_N. The magnetic contribution to the elastic stiffness in the ferrimagnetic state is negative, but only of the order of a percent (Fig. 2).

(iii) The shear stiffness C_{44} is much the most strongly magnetic-field-dependent elastic stiffness in $Tb_3Fe_5O_{12}$. This arises from the first-order magnetoelastic interaction, the magnetoelastic coefficient b_{2323}, which couples components of the magnetic moment to C_{44}-type (η_{ij}, $i \neq j$) strain, being much larger than b_{1111}, which couples to $[(C_{11}-C_{12})/2]$-type ($\eta_{ii}-\eta_{jj}$) strains.

(iv) For a magnetic field applied in a direction at an angle θ to the [110] direction in $Tb_3Fe_5O_{12}$, the change in velocity of the shear elastic mode propagated in the [110] direction and polarized [1$\bar{1}$0] has an orientation dependence consistent with the first-order magnetoelastic interaction.

(v) The mean long-wavelength acoustic-mode gamma γ^{el} for $Tb_3Fe_5O_{12}$ is about twice as large as that of YAG and also substantially larger than that of YIG (Table I). Hence the acoustic-mode vibrational anharmonicities are appreciably larger for $Tb_3Fe_5O_{12}$ than for the other two garnets.

(vi) The elastic stiffness tensor components and their hydrostatic pressure derivatives for a number of rare-earth iron and aluminum garnet crystals (and including those of yttrium and plutonium) have been determined by an atomistic simulation approach (Tables II and III). The elastic stiffness tensor components C_{11}, C_{12}, and C_{44} or of the adiabatic bulk modulus B^S (or of their pressure derivatives) calculated theoretically do not vary substantially through this sequence of garnets. Most garnets have not yet been studied experimentally, but the theoretical calculations are in reasonable agreement with the experimental data for those which have.

(vii) The calculated mean acoustic Grüneisen parameters γ^{el} are all between 0.7 and 0.9 (Table III). The iron garnets have larger Grüneisen parameters (and hence more pronounced vibrational anharmonicity) than the aluminum garnets.

(viii) For YAG, which does not contain magnetic ions, the value of γ^{el} determined theoretically agrees with the experimental quantity, but for $Tb_3Fe_5O_{12}$, in which there are magnetic ions on each cation site, the theoretical γ^{el} is much smaller than that determined experimentally. The implication is that there is a magnetic contribution to the potential and to the acoustic-mode vibrational anharmonicity for $Tb_3Fe_5O_{12}$ and it is likely to occur in other magnetic rare-earth garnets.

[1] M. A. Gilleo, in *Ferromagnetic Materials,* edited by E. P. Wohlfarth (North-Holland, Amsterdam, 1980), Vol. 2, p. 3.

[2] M. Lahoubi, M. Guillot, A. Marchand, E. Roudault, and F. Tcheou, IEEE Trans. Magn. Magn. **MAG-20**, 1518 (1984).

[3] P. J. Flanders, T. Egami, E. M. Gyorgy, and L. G van Uitert, J. Appl. Phys. **49**, 1978 (1978).

[4] Nguyen Hy Hau, P. Porcher, Tran Khahn Vien, and B. Pajot, J. Phys. Chem. Solids **47**, 83 (1986).

[5] S. Ida, Phys. Lett. **6**, 165 (1963).

[6] P. J. Flanders, R. F. Pearson, and J. L. Page, Br. J. Appl. Phys. **17**, 839 (1966).

[7] F. Sayetat, J. Appl. Phys. **46**, 3619 (1975).

[8] F. Sayetat, J. Magn. Mater. **58**, 334 (1986).

[9] H. L. Alberts, J. Phys. Chem. Solids **41**, 1161 (1980).

[10] H. L. Alberts, S. B. Palmer, and C. Patterson, J. Phys. C **21**, 271 (1988).

[11] R. C. LeCraw and T. Kasuya, Phys. Rev. **130**, 50 (1963).

[12] D. E. Eastman, J. Appl. Phys. **37**, 2312 (1966).

[13] Y. K. Yogurtçu, A. J. Miller, and G. A. Saunders, J. Phys. C **13**, 6585 (1980).

[14] N. Soga, J. Geophys. Res. **72**, 4227 (1967).

[15] R. N. Thurston and K. Brugger, Phys. Rev. **123**, 1535 (1964).

[16] F. Bertaut and R. Pauthenet, Proc. Inst. Electr. Eng. B **104**, 261 (1957).

[17] O. P. Kvashnina, A. M. Kapitonov, E. M. Smokotin, and A. G. Titova, Fiz. Tverd. Tela (Leningrad) **26**, 2408 (1984).

[18] D. E. Eastman, Phys. Rev. **148**, 530 (1966).

[19] W. P. Mason, Phys. Rev. **82**, 715 (1951).

[20] R. C. LeCraw and R. L. Comstock, in *Physical Acoustics,* edited by W. P. Mason (Academic, New York, 1965), Vol. IIIB,

p. 127.
[21]K. Brugger and T. C. Fritz, Phys. Rev. **157**, 524 (1967).
[22]G. D. Price and S. C. Parker, Phys. Chem. Miner. **10**, 209 (1984).
[23]G. V. Lewis and C. R. A. Catlow, J. Phys. C **18**, 1149 (1985).
[24]A. Wall, G. D. Price, and S. C. Parker, Mineral. Mag. **50**, 693 (1986).
[25]C. R. A. Catlow and A. M. Stoneham, J. Phys. C **16**, 4321 (1983).
[26]A. N. Cormack, G. V. Lewis, S. C. Parker, and C. R. A. Catlow, J. Phys. Chem. Solids **49**, 53 (1988).
[27]S. C. Parker and G. D. Price, Physica B **131**, 290 (1985).
[28]S. C. Parker and G. D. Price, Adv. Solid State Chem. **1**, 295 (1989).
[29]T. H. K. Barron and M. L. Klein, Proc. Phys. Soc. **85**, 523 (1965).
[30]R. F. S. Hearmon, in *Elastic, Piezoelectric, Pyroelastic, Piezooptic, Electrooptic Constants and Nonlinear Dielectric Susceptibilities of Crystals, Landolt-Börnstein (New Series),* edited by K.-H. Hellwege (Springer-Verlag, Berlin, 1979), Vol. 11.